Biogeosciences

Modelling nitrification inhibitor effects on N$_2$O emissions after fall- and spring-applied slurry by reducing nitrifier NH$_4^+$ oxidation rate

Robert F. Grant, Sisi Lin, and Guillermo Hernandez-Ramirez

Department of Renewable Resources, University of Alberta, Edmonton, AB, T6G 2E3, Canada

Correspondence: Robert F. Grant (rgrant@ualberta.ca)

Abstract. Reductions in N$_2$O emissions from nitrification inhibitors (NI) are substantial but remain uncertain because measurements of N$_2$O emissions are highly variable and discontinuous. Mathematical modelling may offer an opportunity to estimate these reductions if the processes causing variability in N$_2$O emissions can be accurately simulated. In this study, the effect of NI was simulated with a simple, time-dependent algorithm to slow NH$_4^+$ oxidation in the ecosystem model *ecosys*. Slower nitrification modelled with NI caused increases in soil NH$_4^+$ concentrations and reductions in soil NO$_3^-$ concentrations and in N$_2$O fluxes that were consistent with those measured following fall and spring applications of slurry over 2 years from 2014 to 2016. The model was then used to estimate direct and indirect effects of NI on seasonal and annual emissions. After spring slurry applications, NI reduced N$_2$O emissions modelled and measured during the drier spring of 2015 (35 % and 45 %) less than during the wetter spring of 2016 (53 % and 72 %). After fall slurry applications, NI reduced modelled N$_2$O emissions by 58 % and 56 % during late fall in 2014 and 2015 and by 8 % and 33 % during subsequent spring thaw in 2015 and 2016. Modelled reductions were consistent with those from meta-analyses of other NI studies. Simulated NI activity declined over time so that reductions in N$_2$O emissions modelled with NI at an annual timescale were relatively smaller than those during emission events. These reductions were accompanied by increases in NH$_3$ emissions and reductions in NO$_3^-$ losses with NI that caused changes in indirect N$_2$O emissions. With further parameter evaluation, the addition of this algorithm for NI to ecosys may allow emission factors for different NI products to be derived from annual N$_2$O emissions modelled under diverse site, soil, land use and weather.

1 Introduction

Nitrification inhibitors (NI) have frequently been found to reduce N$_2$O emissions from fertilizer and slurry applications in agricultural fields. In a meta-analysis of field experiments conducted for 2008, Akiyama et al. (2010) found average reductions of 38 ± 6 % in N$_2$O emissions from NI, with some variation attributed to land use type and emission rates. Similar average reductions of 35 %–40 % were reported in more recent meta-analyses by Ruser and Schulz (2015), Gilsanz et al. (2016), and Gao and Bian (2017). However the magnitudes of these reductions are uncertain because they vary with the rate and timing of fertilizer or slurry application, with land use and ecosystem type (Akiyama et al., 2010), and with application method (Zhu et al., 2016). These magnitudes are also uncertain because measurements of the N$_2$O emissions on which they are based are highly variable temporally and spatially and difficult to sustain over the annual time periods needed to estimate NI reductions.
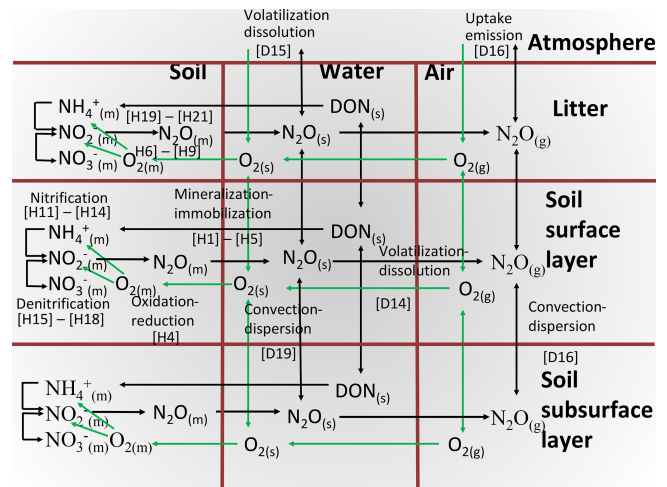
The effects of NI on N$_2$O emissions are attributed to inhibition of ammonia monooxygenase, which slows the oxidation of NH$_4^+$ to NO$_2^-$ during nitrification (Subbarao et al., 2006) and hence slows the reduction of NO$_2^-$ to N$_2$O during nitrifier denitrification. The consequent slowing of NO$_2^-$ oxidation to NO$_3^-$ would also slow the reduction of NO$_3^-$ to N$_2$O during denitrification. The effectiveness of NI has been found to decline over time due to mineralization, adsorption and volatilization, depending on NI formulation. The rate of this decline varies among NI products and soil types and increases with soil temperature (Guardia et al., 2018).

The great majority of the studies included in meta-analyses of NI effects on N$_2$O emissions were conducted following fertilizer or slurry application on warm soils in spring or

summer (e.g. Akiyama et al., 2010). The effectiveness of NI with fall applications of fertilizer or slurry on cold soils has thus far received very limited attention (Ruser and Schulz, 2015), although in cold climates N_2O emissions during the spring thaw following fall applications may exceed those during late spring and summer following spring applications (Lin et al., 2018). Emissions during spring thaw were attributed by Wagner-Riddle and Thurtell (1998) to soil NO_3–N concentrations exceeding $20\,\mathrm{mg\,kg}^{-1}$ generated by fall-applied slurry that contributed to total N_2O emissions exceeding $0.2\,\mathrm{g\,N\,m}^{-2}$ measured between January and April of the following year. Large N_2O emissions measured in late winter were attributed by Dungan et al. (2017) to labile N not used by soil microorganisms during the previous fall and winter that was actively metabolized when the soils began to warm in early March. Interannual differences in spring thaw emission events after fall slurry applications were related by Kariyapperuma et al. (2012) to those in total soil mineral N content in the upper 15 cm of the soil profile during spring thaw. The effects of NI on N_2O emissions during spring thaw will therefore depend on the persistence with which NI reduce nitrification in cold soils during fall and winter and thereby alter mineral N concentrations during the following spring.

Reductions in N_2O emissions directly caused by slower nitrification with NI may be partially offset by increases in indirect N_2O emissions from increasing NH_3 emissions caused by greater soil NH_4^+ concentrations (Lam et al., 2017; Qiao et al., 2015). NI may also decrease indirect N_2O emissions by reducing NO_3^- concentrations and hence leaching. Both direct and indirect effects of NI on N_2O emissions must be considered when estimating effects of NI on total N_2O emissions.

The Intergovernmental Panel on Climate Change (IPCC) Tier 3 methodology for estimating N_2O emissions under diverse climates, soils, fertilizers and land uses includes the use of comprehensive, process-based mathematical models of terrestrial C, N, and water and energy cycling (IPCC, 2019). Although NI effects on nitrification have been added to some existing process models (Cui et al., 2014; Del Grosso et al., 2009; Li et al., 2020), testing of modelled NI effects on N_2O emissions against measurements remains limited to brief periods following soil N amendments (e.g. Giltrap et al., 2011). The mathematical model ecosys explicitly represents the key processes in nitrification (Grant, 1994), denitrification (Grant, 1991) and associated N_2O emissions (Grant, 1995) and has been tested against measurements of N_2O emissions using micrometeorological methods and manual and automated chambers (Grant and Pattey, 1999, 2008; Grant et al., 2006, 2016; Metivier et al., 2009). In this study, we propose that applying a time-dependent reduction of NH_4^+ oxidation rates during nitrification will enable ecosys to simulate the time course of reductions in N_2O emissions with NI measured after fall and spring applications of dairy slurry in a field experiment. The model is then used to estimate the di-

Figure 1. Key transformations governing N_2O emissions as represented in ecosys. Expressions in square brackets refer to equations in the Supplement, as described in Sect. 2.

rect and indirect effects of NI on annual N_2O emissions with fall and spring slurry applications as required for IPCC Tier 3 methodology and how these effects would change with alternative tillage practices and timings of slurry application.

2 Model development

2.1 General overview

The hypotheses for oxidation–reduction reactions involving N_2O, and the aqueous and gaseous transport of their substrates and products, are represented in Fig. 1 and described in further detail below. These hypotheses function within a comprehensive model of soil C, N and P transformations, which is coupled to models of soil water, heat and solute transport in surface litter and soil layers. These models function within the comprehensive ecosystem model ecosys. Key transformations that drive N_2O emissions are described in Sect. 2.2 to 2.8 below, and modifications of these transformations to simulate nitrification inhibition are described in Sect. 2.9. References to equations and definitions in Sect. 2.2 to 2.8 and given in Supplement S1, S3, S4, S5 and S8 (Table 1) are provided for those interested in model methodology but are not needed for a general understanding of model behaviour.

2.2 Mineralization and immobilization of ammonium by microbial functional types

Heterotrophic microbial functional types (MFTs) m (obligately aerobic bacteria, obligately aerobic fungi, facultatively anaerobic denitrifiers, anaerobic fermenters, acetotrophic methanogens, and obligately aerobic and anaerobic non-symbiotic diazotrophs) are associated with each organic

Table 1. List of sections in the Supplement.

Supplement	Title	Equations
S1	Microbial C, N and P transformations	[A1]–[A39]
S2	Soil–plant water relations	[B1]–[B14]
S3	Gross primary productivity, autotrophic respiration, growth and litterfall	[C1]–[C53]
S4	Soil water, heat, gas and solute fluxes	[D1]–[D21]
S5	Solute transformations	[E1]–[E57]
S6	Symbiotic N$_2$ fixation	[F1]–[F26]
S7	CH$_4$ production and consumption	[G1]–[G27]
S8	Inorganic N transformations	[H1]–[H21]

substrate i (i is manure, coarse woody plant residue, fine non-woody plant residue, particulate organic matter or humus). Autotrophic MFTs n (aerobic NH$_4^+$ and NO$_2^-$ oxidizers, aerobic methanotrophs, and hydrogenotrophic methanogens) are associated with inorganic substrates. These MFTs grow [A25] with energy generated from oxidation of dissolved organic C (DOC) by heterotrophs [H2, H10], of acetate by acetotrophic methanogens, of mineral N (NH$_4^+$ and NO$_2^-$) [H11, H15] by nitrifiers, of CH$_4$ by methanotrophs [G7] or of H$_2$ by hydrogenotrophic methanogens [G12], coupled with reduction of e$^-$ acceptors O$_2$ [H4, G22], acetate [G8], NO$_x$ [H7–H9] and CO$_2$ [G13]. These MFTs decay according to first-order rate constants [A23], with internal recycling of resources (C, N, P) from structural to nonstructural components j (j is labile, recalcitrant, nonstructural) varying with nonstructural C : N : P ratios [A24], the decay products of which form humus C, N and P [A35, A36]. Each MFT seeks to maintain a set nonstructural C : N : P ratio by mineralizing NH$_4^+$ and H$_2$PO$_4^-$ [H1a] from, or by immobilizing NH$_4^+$, NO$_3^-$ and H$_2$PO$_4^-$ [H1b, H1c] into, its nonstructural N and P components. These transformations control the exchange of N and P between organic and inorganic states, and of O$_2$ between aqueous and gaseous states, and hence affect the availability of substrates and e$^-$ acceptors for nitrification and denitrification.

2.3 Oxidation of DOC and reduction of oxygen by heterotrophs

N$_2$O is generated when demand for e$^-$ acceptors from oxidation by aerobic heterotrophs and autotrophs (Sect. 2.2) exceeds supply from O$_2$, requiring explicit modelling of O$_2$ transport and uptake and consequent O$_2$ constraints to oxidation–reduction reactions (Fig. 1). Constraints on heterotrophic oxidation of DOC imposed by O$_2$ uptake are solved in four steps:

1. DOC oxidation by heterotrophs under non-limiting O$_2$ is calculated from specific oxidation rates multiplied by active biomasses and an Arrhenius function of T_s [A6] used for all microbial transformations, constrained by DOC concentration [H2].

2. O$_2$ reduction to H$_2$O under non-limiting O$_2$ (O$_2$ demand) by aerobic heterotrophs is calculated from step 1 using a set respiratory quotient [H3].

3. O$_2$ reduction to H$_2$O under ambient O$_2$ is calculated from radial O$_2$ diffusion through water films with thicknesses determined by soil water potential [H4a] coupled with active uptake at heterotroph surfaces driven by step 2 [H4b]. Diffusion and uptake are sustained by O$_2$ transfer through soil aqueous and gaseous phases controlled by soil water- and air-filled porosity governed by freezing, thawing and transfer of soil water [D14–D20]. O$_2$ diffusion and active uptake are calculated for each heterotrophic population associated with each organic substrate, allowing [H4] to calculate lower O$_2$ concentrations at microbial surfaces (O$_{2m}$) associated with more biologically active substrates (e.g. manure, litter). Localized zones of low O$_2$ concentration (hotspots) are thereby simulated when O$_2$ uptake by any aerobic MFT is constrained by O$_2$ diffusion to that functional type. O$_2$ uptake by each heterotrophic MFT is affected by competition for O$_2$ uptake with other heterotrophs, nitrifiers, roots and mycorrhizae, calculated from its biological O$_2$ demand relative to those of other aerobic functional types.

4. DOC oxidation to CO$_2$ under ambient O$_2$ is calculated from steps 2 and 3 [H5]. The energy yield of DOC oxidation with O$_2$ reduction drives the uptake of additional DOC for construction of microbial biomass $M_{i,h}$ according to construction energy costs of each heterotrophic functional type [A21]. Energy costs of denitrifiers are slightly larger than those of obligately aerobic heterotrophs, placing denitrifiers at a small competitive disadvantage for growth and hence DOC oxidation under non-limiting O$_2$.

2.4 Oxidation of DOC and reduction of nitrate, nitrite and nitrous oxide by denitrifiers

N$_2$O may be both the product and substrate of NO$_x$ reduction coupled with DOC oxidation by denitrifiers. Constraints

imposed by NO$_3^-$ availability on denitrifier DOC oxidation are solved in five steps:

1. NO$_3^-$ reduction to NO$_2^-$ by heterotrophic denitrifiers under non-limiting NO$_3^-$ is calculated from demand for e$^-$ acceptors by denitrifiers for DOC oxidation to CO$_2$ but not met from O$_2$ reduction to H$_2$O because of diffusion limitations to the O$_2$ supply (Sect. 2.3, step 3). This unmet demand is transferred to NO$_3^-$ [H6].

2. NO$_3^-$ reduction to NO$_2^-$ under ambient NO$_3^-$ is calculated from step 1, accounting for relative concentrations and affinities of NO$_3^-$ and NO$_2^-$ [H7].

3. NO$_2^-$ reduction to N$_2$O under ambient NO$_2^-$ is calculated from demand for e$^-$ acceptors not met by NO$_3^-$ reduction in step 2, accounting for relative concentrations and affinities of NO$_2^-$ and N$_2$O. This unmet demand is transferred to NO$_2^-$ [H8].

4. N$_2$O reduction to N$_2$ under ambient N$_2$O is calculated from demand for e$^-$ acceptors not met by NO$_2^-$ reduction in step 3 and hence transferred to N$_2$O [H9].

5. Additional energy yield from DOC oxidation to CO$_2$ enabled by NO$_x$ reduction in steps 2, 3 and 4 is added to that enabled by O$_2$ reduction from [H5], which drives additional DOC uptake for construction of $M_{i,\mathrm{n}}$. This additional uptake offsets the disadvantage incurred by the larger construction energy costs of denitrifiers (Sect. 2.3, step 4).

2.5 Oxidation of ammonium and reduction of oxygen by nitrifiers

N$_2$O may also be generated by reduction of NO$_2^-$ coupled with oxidation of NH$_4^+$ by autotrophic nitrifiers. Constraints on nitrifier oxidation of NH$_4^+$ imposed by O$_2$ uptake are solved in four steps:

1. Oxidation of NH$_4^+$ (in dynamic equilibrium with NH$_3$ [E24]) under non-limiting O$_2$ is calculated from a specific oxidation rate multiplied by active biomass and an Arrhenius function of T_s and constrained by NH$_4^+$ and CO$_2$ concentrations [H11].

2. O$_2$ reduction to H$_2$O under non-limiting O$_2$ (O$_2$ demand) is calculated from step 1 using set respiratory quotients [H12].

3. O$_2$ reduction to H$_2$O under ambient O$_2$ is calculated from radial O$_2$ diffusion through water films of thickness determined by soil water potential [H13a] coupled with active uptake at nitrifier surfaces driven by step 2 [H13b]. O$_2$ uptake by nitrifiers is affected by competition for O$_2$ uptake with heterotrophic DOC oxidizers, roots and mycorrhizae, calculated from its biological O$_2$ demand relative to those of other aerobic functional types.

4. NH$_4^+$ oxidation to NO$_2^-$ under ambient O$_2$ is calculated from steps 2 and 3 [H14]. The energy yield of NH$_4^+$ oxidation drives the fixation of CO$_2$ for construction of microbial biomass $M_{i,\mathrm{n}}$ according to nitrifier construction energy costs.

2.6 Oxidation of nitrite and reduction of oxygen by nitrifiers

Constraints on nitrifier oxidation of NO$_2^-$ to NO$_3^-$ imposed by O$_2$ uptake [H15–H18] are solved in the same way as those of NH$_4^+$ to NO$_2^-$ [H11–H14]. The energy yield of NO$_2^-$ oxidation drives the fixation of CO$_2$ for construction of microbial biomass $M_{i,\mathrm{o}}$ according to nitrifier construction energy costs.

2.7 Oxidation of ammonium and reduction of nitrite by nitrifiers

In both nitrifier and denitrifier processes, N$_2$O is generated from reduction of NO$_2^-$, the availability of which is controlled by NO$_2^-$ oxidation (Sect. 2.6). Under low O$_2$ concentrations NO$_2^-$ oxidation is suppressed [H18], favouring NO$_2^-$ reduction. Constraints on nitrifier oxidation of NH$_4^+$ imposed by NO$_2^-$ availability are solved in three steps:

1. NO$_2^-$ reduction to N$_2$O under non-limiting NO$_2^-$ is calculated from e$^-$ acceptors demanded by NH$_4^+$ oxidation to NO$_2^-$ but not met by O$_2$ for reduction to H$_2$O because of diffusion limitations to O$_2$ supply and hence transferred to NO$_2^-$ [H19].

2. NO$_2^-$ reduction to N$_2$O under ambient NO$_2^-$ and CO$_2$ is calculated from step 1 [H20], competing for NO$_2^-$ with denitrifiers [H8] and nitrifiers [H18].

3. Energy yield from additional NH$_4^+$ oxidation to NO$_2^-$ enabled by NO$_2^-$ reduction in step 2 [H21] is added to that enabled by O$_2$ reduction from step 4 in Sect. 2.5 [H14], which drives the fixation of additional CO$_2$ for construction of $M_{i,\mathrm{n}}$.

2.8 Uptake of ammonium and reduction of oxygen by roots and mycorrhizae

NH$_4^+$ oxidation and O$_2$ reduction by nitrifiers compete for substrates with NH$_4^+$ uptake and O$_2$ reduction by other MFTs and by roots and mycorrhizae.

1. NH$_4^+$ uptake by roots and mycorrhizae under non-limiting O$_2$ is calculated from mass flow and radial diffusion between adjacent roots and mycorrhizae [C23a] coupled with active uptake at root and mycorrhizal surfaces [C23b]. Active uptake is subject to product inhibition by root nonstructural N : C ratios [C23g], where nonstructural N is the active uptake product, and nonstructural C is the CO$_2$ fixation product transferred to roots and mycorrhizae from the canopy.

2. O$_2$ reduction to H$_2$O under non-limiting O$_2$ is calculated from O$_2$ demands for NH$_4^+$ uptake in step 1 and for oxidation of root and mycorrhizal nonstructural C for root maintenance and growth using a set respiratory quotient [C14e].

3. O$_2$ reduction to H$_2$O under ambient O$_2$ is calculated from mass flow and radial diffusion between adjacent roots and mycorrhizae [C14d] coupled with active uptake at root and mycorrhizal surfaces driven by step 2 [C14c]. O$_2$ uptake by roots and mycorrhizae is also affected by competition with O$_2$ uptake by heterotrophic DOC oxidizers, and autotrophic nitrifiers, calculated from their biological O$_2$ demands relative to those of other populations.

4. Oxidation of root and mycorrhizal nonstructural C to CO$_2$ under ambient O$_2$ is calculated from steps 2 and 3 [C14b].

5. NH$_4^+$ uptake by roots and mycorrhizae under ambient O$_2$ is calculated from steps 1, 2, 3 and 4 [C23b].

2.9 Nitrification inhibition

For this study, NI were assumed to reduce specific rates of NH$_4^+$ oxidation by nitrifiers in step 1 in Sect. 2.5, thereby simulating inhibition of ammonia monooxygenase (Subbarao et al., 2006). This reduction was represented by a time-dependent scalar I:

$$I_{t_1} = I_{t-1_1} - I_{t-1_1} \cdot R_I \cdot f_{T_{s1}}, \tag{1}$$

where t is the current time step (h), $t - 1$ is the previous time step (h), I is the inhibition (initialized to 1.0 at $t = 0$ at the time of application), R_I is the rate constant for decline of I representing NI degradation (set to 2.0×10^{-4} h^{-1} for more persistent NI such as 3,4-dimethylpyrazole phosphate – DMPP – and to 1.0×10^{-3} h^{-1} for less persistent NI such as nitrapyrin; Ruser and Schulz, 2015), f_{T_s} is an Arrhenius function of soil temperature (T_s) used to simulate T_s effects on microbial activity ([A6] in step 1, Sect. 2.3), and l is the soil layer in which NI are present. The values of R_I and f_{T_s} for DMPP were selected to give time and temperature dependencies of DMPP activity following application inferred from incubation studies by Guardia et al. (2018). Model results for NI presented below are those using the smaller R_I for DMPP unless stated as those using the larger R_I for nitrapyrin.

Specific rates of NH$_4^+$ oxidation (step 1, Sect. 2.5) with NI was calculated as

$$X'_{NH4_{1}} = X''_{NH4_1} \cdot \left(1.0 - I_{t_1} / \left(1.0 + [NH_4^+]_1 / K_{iNH4}\right)\right), \tag{2}$$

where X'_{NH4} and X''_{NH4} are specific NH$_4^+$ oxidation rates with and without NI (g N g nitrifier C^{-1} h^{-1}), [NH$_4^+$] is the

aqueous NH$_4^+$ concentration (g N m^{-3} in dynamic equilibrium with [NH$_3$]), and K_{iNH4} is an inhibition constant set at 7000 g N m^{-3} to reduce inhibition at very large [NH$_4^+$] as suggested in Janke et al. (2019). These rates were used to calculate nitrification rates [H11]:

$$X_{NH4_{1}} = X'_{NH4_1} M_{nl} f_{T_{s1}} \left\{ [NH_4^+]_1 / \left([NH_4^+]_1 + K_{NH4}\right) \right\}$$

$$\left\{ [CO_2s]_1 / \left([CO_2s]_1 + K_{CO_2}\right) \right\}, \tag{3}$$

where X_{NH4t} is the nitrification rate (g N m^{-2} h^{-1}), M_n is the nitrifier biomass (g C m^{-2}), and K_{NH4} and K_{CO_2} are half-saturation constants for aqueous NH$_4^+$ and CO$_2$ (g N and C m^{-3}). The NI in Eq. (1) slows X'_{NH4t} in Eq. (2) and thereby X_{NH4t} in Eq. (3) and hence slows NO$_2^-$ production from nitrification (step 4, Sect. 2.5) and thereby N$_2$O production from nitrification (step 2, Sect. 2.7) and denitrification (step 3, Sect. 2.4). By slowing X_{NH4t} in Eq. (3), NI also reduce nitrification energy yield and hence M_n growth, biomass [A25] and O$_2$ uptake [H13], thereby further reducing N$_2$O production.

3 Field experiment

3.1 Site description and experimental design

An experiment was established on a Black Chernozem (Table 2) under barley (*Hordeum vulgare* L.) silage from 2014 to 2016 on a level site at the South Campus Farm in Edmonton, AB, Canada (53°29′30″ N, 113°31′53″ W). The experimental design was an incomplete split plot (main plot: fall vs. spring application of dairy slurry; split plot: control vs. NI treatments) on plots 2.4 m in width and 6.1 m in length with three replicates. The NI products ENTEC (EuroChem Agro, Mannheim, Germany) and the eNtrench nitrogen stabilizer (Dow Chemical Company, Dow AgroSciences, Calgary, AB, Canada) were mixed with the slurry immediately before application to provide 0.4 kg ha^{-1} of the active ingredient with slurry injection of 56.17 m^3 ha^{-1} at 12.7 to 15.2 cm (average 14 cm) depth and 28 cm spacing. Measured concentrations of NH$_4^+$ and of organic N and C in each slurry application were used to calculate rates of NH$_4^+$, organic N and organic C amendments (Table 3). Soil NH$_4^+$ concentrations were measured from 0 to 10 cm every 2–3 weeks between spring thaw and autumn freezing in 2014, 2015 and 2016. Further details of this field experiment are given in Lin et al. (2018).

Weather data (radiation, air temperature – T_a, humidity, wind speed and precipitation) were recorded hourly from 2012 to 2016 at the South Campus Farm. During the first experimental year (16 September 2014 to 15 September 2015) T_a remained 1–2 °C higher than historical (1981–2010) averages (Lin et al., 2018; Table 4). Precipitation was slightly higher than historical averages during autumn and winter but

Table 2. Key soil properties of the Black Chernozem soil at the South Campus Farm used in ecosys. SOC is soil organic carbon, and SON is soil organic nitrogen.

Depth	BD	FC	WP	K_{sat}*	Sand	Silt	Clay	pH	SOC	SON
m to bottom	$Mg\,m^{-3}$	$m^3\,m^{-3}$		$mm\,h^{-1}$	$g\,kg^{-1}$ mineral soil				$g\,kg^{-1}$ soil	
0.01	1.15	0.34	0.15	18.0	280	450	270	6.3	57.1	5.74
0.025	1.15	0.34	0.15	18.0	280	450	270	6.3	57.1	5.74
0.05	1.15	0.34	0.15	18.0	280	450	270	6.3	57.1	5.74
0.10	1.15	0.34	0.15	18.0	280	450	270	6.3	57.1	5.74
0.15	1.35	0.34	0.15	18.0	280	450	270	6.3	40.7	3.80
0.30	1.40	0.34	0.15	7.5	250	470	280	6.3	40.7	3.80
0.60	1.50	0.35	0.17	2.5	270	420	310	7.1	3.2	0.3
0.90	1.50	0.35	0.17	2.5	270	420	310	7.1	3.2	0.3
1.20	1.50	0.35	0.17	2.5	270	420	310	7.1	3.2	0.3
1.50	1.50	0.35	0.17	2.5	270	420	310	7.1	3.2	0.3

* From Saxton et al. (1986).

Table 3. Plant and soil management schedule at the Edmonton South Campus Farm.

Year	Date	Management	Amount			
			Urea $g\,N\,m^{-2}$	NH_4^+ $g\,N\,m^{-2}$	Organic N $g\,N\,m^{-2}$	Organic C $g\,C\,m^{-2}$
2014	15 May	Fertilizer	7.2			
	15 May	Planting				
	21 Aug	Harvest				
	30 Sep	Fall slurry		21.7	16.4	229.4
2015	11 May	Planting				
	12 May	Spring slurry		19.4	20.5	176.9
	28 Jul	Harvest				
	7 Oct	Fall slurry		21.3	19.0	198.5
2016	14 May	Planting				
	16 May	Spring slurry		27.2	18.6	227.5
	15 Aug	Harvest				

was about one-half those during spring and summer. During the second experimental year (16 September 2015 to 15 September 2016), T_a was higher than that of the first year during winter and early spring and similar during late spring and summer. However precipitation during the second year was lower from autumn to early spring and much higher during late spring and summer.

3.2   N₂O flux measurements

N₂O fluxes were measured at 3 h intervals from as soon as field conditions allowed after spring thaw to late summer during both experimental years with automated chambers (height of 26 cm, area of $0.216\,m^2$) connected by 0.5 cm i.d. tubes to a FTIR gas analyser (GASMET model CX4025, Temet Instruments, Finland) through which air flow was maintained at $5.1\,L\,min^{-1}$. During each 20 min measurement period, the chambers remained open for the first 5 min to re-store ambient N₂O concentrations in the gas analyser, after which chambers were closed and N₂O concentrations were measured at 10 Hz and averages recorded at 1 min intervals. Concentrations during the first minute after closure were discarded, and those during the following 14 min were used to calculate fluxes using linear regression with an acceptance criterion of $R^2 \geq 0.85$. Based on the analytical precision of the gas analyser, the N₂O flux detection limit was determined to be $\pm 0.03\,mg\,N\,m^{-2}\,h^{-1}$.

N₂O emissions were also measured once or twice per week from spring thaw to autumn freezing during both experimental years with manually operated chambers as described in Lin et al. (2018). The time required for installation of the automated chambers after snowmelt limited their ability to measure N₂O emissions during spring thaw so that measurements from the manually operated chambers were used to evaluate emissions during these periods.

Table 4. Average temperatures and total precipitation measured at the Edmonton South Campus Farm during autumn–winter, winter–spring and spring–summer in 2014–2015 and 2015–2016.

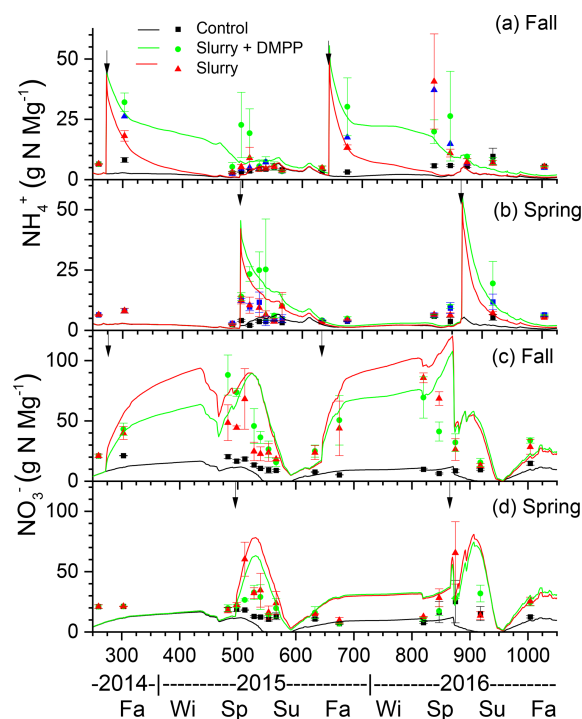|	2014	2015		2014–2015	2015	2016		2015–2016
From	16 Sep	1 Jan	1 May	Average	16 Sep	1 Jan	1 May	Average
To	31 Dec	30 Apr	15 Sep	or total	31 Dec	30 Apr	15 Sep	or Total
Temp. (°C)	0.4	−1.8	16.0	5.6	0.8	0.1	15.8	6.3
Precip. (mm)	50	75	195	320	41	38	402	481

4 Model experiment

4.1 Model spin-up

To simulate site conditions prior to the experiment, ecosys was initialized with the properties of the Black Chernozem, simulated as a one-dimensional profile (Table 2) with surface water runoff and subsurface water exchange with a water table at 1.2 m depth. The model was run from model dates 1 January 1992 to 31 December 2013 under a repeating 5-year sequence of weather data (radiation, air temperature – T_a, humidity, wind speed and precipitation) recorded hourly from 2012 to 2016 at the South Campus Farm. During each year of the spin-up run, barley was planted, fertilized and harvested as silage to reproduce land use practices reported from the field site.

4.2 Model runs

The spin-up run was extended from 1 January 2014 to 31 December 2016 under weather data recorded from 2014 to 2016 with the land use schedules and practices from the field site (Table 3). Each modelled slurry application was added to the soil layer, the depth of which corresponded to that of slurry injection in the field experiment (14 cm). Modelled applications were accompanied by addition of water corresponding to the volume and depth of the application (5.6 mm from 56.17 m^3 ha^{-1} at 14 cm in Sect. 3.1), and by tillage using a coefficient for surface litter incorporation and soil mixing of 0.2 to the depth of application (14 cm), based on field observations. A control run was also conducted in which no slurry applications were modelled. For all silage harvests, cutting height and harvest efficiency were set to 0.15 m and 0.9 so that 0.9 of all plant material above 0.15 m was removed as yield. Concentrations of NH$_4^+$ and NO$_3^-$, and N$_2$O emissions modelled during key emission events, were compared with measured values (Sect. 3.1 and 3.2), and modelled emissions were then aggregated into seasonal and annual values.

There is some flexibility in the timing of fall slurry application between crop harvest in late summer and soil freezing in early November. To examine how timing of fall slurry application would affect subsequent N$_2$O emissions with and without NI, fall slurry application dates were advanced or delayed by 2 weeks from those in Table 3, and effects on spring

Figure 2. Soil NH$_4^+$ and NO$_3^-$ concentrations measured (symbols) and modelled (lines) at 0–10 cm depth following applications of dairy slurry without and with DMPP. Arrows indicate dates of application. (Fa – fall; Wi – winter; Sp – spring; Su – summer.)

and annual N$_2$O emissions were evaluated. To examine how increased tillage during slurry application would affect subsequent N$_2$O emissions with and without NI, coefficients for surface litter incorporation and soil mixing to the depth of slurry application were raised from 0.2 to 0.5 and 0.8 for fall and spring applications.

5 Results

5.1 NI and soil NH$_4^+$ and NO$_3^-$ concentrations

5.1.1 Fall slurry applications

In the model, NI slowed NH$_4^+$ oxidation (Sect. 2.9, Eq. 3) so that declines in NH$_4^+$ concentrations modelled and mea-

sured after fall and spring slurry applications with NI were slower than those without NI (Fig. 2a), particularly during winter, when declines in inhibition were slowed by low T_s (Sect. 2.9, Eq. 1) following the onset of soil freezing modelled at the depth of slurry injection (DOY 313 in 2014 and DOY 318 in 2015 in Fig. 2a). Overwinter declines in NH$_4^+$ concentrations were slower during the winter of 2015–2016, with lower T_s modelled under less winter precipitation and hence shallower snowpack (Table 4). These slower declines caused larger NH$_4^+$ concentrations to be modelled during the following spring, consistent with measurements (Fig. 2a). The slower declines in NH$_4^+$ concentrations modelled with NI caused slower rises in NO$_3^-$ concentrations following fall slurry applications (Fig. 2c). However slower rises with NI were not always apparent in the measured NO$_3^-$ concentrations.

5.1.2 Spring slurry applications

Declines in NH$_4^+$ concentrations modelled after slurry applications with NI in spring 2015 and 2016 were also slower than after those without NI (Fig. 2b), consistent with higher NH$_4^+$ concentrations measured after spring application with DMPP in both years (Fig. 2b). These slower declines caused slower rises in NO$_3^-$ concentrations to be modelled following spring slurry applications with NI (Fig. 2d).

5.2 NI and soil gas concentrations

5.2.1 Fall slurry applications

In the model, soil ice impeded drainage during spring snowmelt and soil thaw, raising θ_w and lowering θ_g, thereby slowing gas transfers in gaseous phases and gas exchanges between gaseous and aqueous phases (Sect. 2.3, step 3; Fig. 1). Freeze–thaw effects on N$_2$O emissions modelled during early spring are further described in Grant and Pattey (1999). Slower O$_2$ transfers relative to O$_2$ uptake (Sect. 2.3, 2.5 and 2.6) forced reductions in aqueous O$_2$ concentrations (O$_{2s}$) to be modelled during early spring in 2015 (Fig. 3a, b) and 2016 (Fig. 3c, d) following fall slurry applications in 2014 and 2015. Declines in aqueous O$_2$ (O$_{2s}$) were later but more rapid in 2015 than in 2016, following greater winter precipitation and hence greater snowmelt in 2014–2015 (Table 4). Earlier and more persistent declines in O$_{2s}$ were modelled in 2016 because greater θ_i modelled with less thermal insulation under a shallower snowpack reduced or eliminated θ_g during much of the winter. Drainage of meltwater after snowmelt eventually lowered θ_w and raised θ_g, allowing O$_{2s}$ to return to atmospheric equivalent concentrations.

Declines in O$_{2s}$ in slurry-amended treatments drove increases in aqueous N$_2$O concentrations (N$_2$O$_s$; Fig. 3b, d) during winter and early spring (Sect. 2.7, step 1). These rises were similar with and without NI in spite of higher NH$_4^+$

concentrations without NI (Fig. 2a). Rises in θ_g following spring drainage allowed volatilization of N$_2$O from aqueous to gaseous phases, reducing N$_2$O$_s$ and driving N$_2$O emissions modelled during spring thaw.

5.2.2 Spring slurry applications

Declines in O$_{2s}$ modelled after spring slurry application were small during the drier spring of 2015 (Table 4; Fig. 3e) but were greater with lower θ_g during the wetter spring of 2016 (Fig. 3g). During both years, these declines were more rapid with slurry than without but less rapid with NI-amended slurry than with unamended slurry. Greater declines in O$_{2s}$ modelled in 2016 vs. 2015 drove greater increases in N$_2$O$_s$ (Sect. 2.7), particularly without NI, and hence greater emissions of N$_2$O during subsequent declines in N$_2$O$_s$.

5.3 NI and N$_2$O fluxes
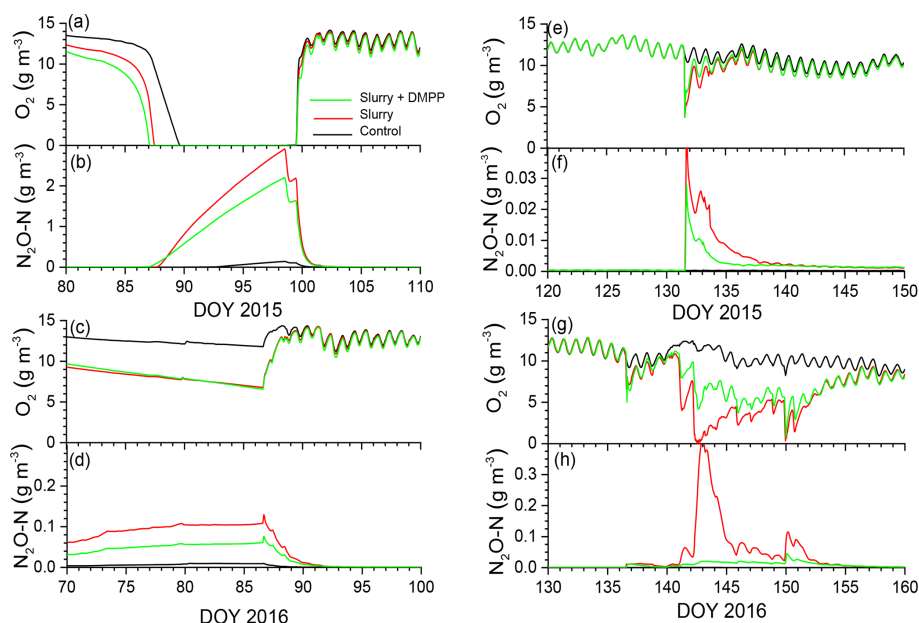
5.3.1 Fall slurry applications

Smaller rises and subsequent declines in N$_2$O$_s$ modelled with NI than without (Fig. 3b) drove smaller N$_2$O emission events modelled during spring thaw in 2015 (Fig. 4a) following slurry application in fall 2014 (Fig. 4b). These events were driven by increases in θ_g during mid-afternoon thawing of near-surface soil but were terminated by loss of θ_g during nighttime refreezing. These events preceded the start of the automated chamber measurements on DOY 102 and so could not be corroborated by them. However measurements with manual chambers earlier in spring 2015 by Lin et al. (2018) indicated that N$_2$O emission events occurred from DOY 85 to 100 that were similar in magnitude although not always in timing with those modelled (Fig. 4b). These measured emissions were smaller with NI than without, consistent with modelled emissions.

The smaller rises and subsequent declines in N$_2$O$_s$ modelled with NI than without in the winter of 2016 (Fig. 3d) drove smaller emission events during thawing and refreezing of near-surface soil in spring 2016 (Fig. 5a) following slurry application in fall 2015 (Fig. 5b). These modelled events preceded the start of automated chamber measurements on DOY 91, but earlier measurements with manual chambers indicated that N$_2$O emission events occurred from DOY 74 to 93. The smaller emission events modelled with NI were consistent with those measured using the manual chambers, although some larger emissions measured with DMPP using the automated chambers from DOY 91 to 102 were not modelled (Fig. 5b). In both years, emissions modelled and measured without slurry remained very small, consistent with low N$_2$O$_s$ (Fig. 3b, f).

5.3.2 Spring slurry applications

Modelled N$_2$O emissions closely followed measured values during a brief emission event following slurry application in

Figure 3. Aqueous concentrations of O$_2$ and N$_2$O modelled at depth of slurry injection (14 cm) during emission events in early spring of **(a, b)** 2015 and **(c, d)** 2016 after fall slurry applications with or without DMPP on DOY 273 in 2014 and DOY 280 in 2015 and later in spring of **(e, f)** 2015 and **(g, h)** 2016 after spring slurry applications on DOY 132 in 2015 and DOY 137 in 2016.

the drier spring of 2015 (Fig. 6a, b), driven by small rises and declines in N$_2$O$_s$ (Fig. 3f). The smaller rise and decline in N$_2$O$_s$ modelled with NI than without drove smaller N$_2$O emissions which declined more rapidly after application than emissions measured with DMPP (Fig. 6b).

Emissions modelled without NI in the wetter spring of 2016 were larger than those in the drier spring of 2015 (Fig. 7a, b), driven by a larger rise and decline in N$_2$O$_s$ with lower θ_g (Fig. 3h). These emissions were suppressed by low θ_g with soil wetting during heavy rainfall on DOY 141–143 shortly after slurry application (Fig. 7a,b) but resumed when θ_g rose with soil drainage thereafter (Fig. 7b). Emissions modelled without NI remained greater than those measured until DOY 150, after which modelled values declined with soil drying while the measured value rose (Fig. 7b). Greater reductions in N$_2$O$_s$ (Fig. 3h) and hence in N$_2$O emissions were modelled with NI after slurry application in the wetter spring of 2016 (Fig. 7b) than in the drier spring of 2015 (Fig. 6b). In both years, emissions modelled and measured without slurry remained very small, consistent with low N$_2$O$_s$ (Fig. 3f, h).

5.4 NI effects on seasonal and annual N$_2$O emissions

5.4.1 Modelled vs. measured N$_2$O emissions after spring slurry applications

Total N$_2$O emissions modelled without NI and with NI using R_I for DMPP or nitrapyrin (Sect. 2.9) were compared with those aggregated from automated chamber measure-

ments over 30 d periods after spring slurry applications in 2015 and 2016 (Table 5). Total emissions modelled and measured without NI were greater during the wetter spring of 2016 than during the drier spring of 2015. Reductions in 30 d emissions modelled and measured with R_I for DMPP and nitrapyrin were greater during the wetter spring in 2016 (53 % and 41 %) than during the drier spring in 2015 (35 % and 30 %). These reductions were somewhat smaller than those measured with DMPP and nitrapyrin in 2016 (72 % and 64 %) and 2015 (45 % and 36 %). Emissions were not measured with automated chambers after fall slurry applications, preventing comparisons with modelled values.

5.4.2 Seasonal and annual N$_2$O emissions modelled after fall and spring slurry applications

Fall slurry applications

NI greatly reduced N$_2$O emissions modelled from fall applications during autumn (16 September–31 December in Table 6) in 2014 and 2015 and slightly reduced N$_2$O emissions modelled during the following winter and early spring (1 January–30 April), but they slightly raised N$_2$O emissions modelled during the following summer (1 May–15 September) in both 2015 and 2016. Annual emissions modelled with NI were reduced from those without NI by 26 % and 38 % in 2014–2015 and 2015–2016 respectively (Table 6). The reduction modelled in 2014–2015 was similar to that of 23 %, estimated for DMPP from manual chamber measurements from 1 October 2014 to 30 September 2015 by Lin et

Table 5. Seasonal N$_2$O emissions measured and modelled during late spring in 2015 and 2016 without slurry (C) or with slurry applied in spring (S) without NI, with nitrapyrin or with DMPP on dates in the field study (Table 3). Negative values denote emissions, and positive values denote uptake.

| Treat. | Amend. | Year | 2015 | 2016 | |
| | | Period | 12 May–11 Jun | 17 May–16 Jun | |
		Measured mg N m^{-2}	Modelled mg N m^{-2}	Measured mg N m^{-2}	Modelled mg N m^{-2}
C			+3	−1	+14	−5
S	None		−88	−89	−160	−153
S	DMPP		−48	−58	−45	−72
S	Nitrapyrin		−56	−62	−57	−91

al. (2018), although the reduction with NI modelled in 2014–2016 was greater than that of 15 %, estimated from manual chamber measurements from 1 October 2015 to 30 September 2016.

Spring slurry applications

Reductions in annual N$_2$O emissions modelled from spring slurry applications with DMPP and nitrapyrin occurred almost entirely during late spring and summer (1 May–15 September in Table 6). These reductions were 22 % and 40 % from those modelled without NI in 2014–2015 and 2014–2016 respectively (Table 6). The reduction modelled with NI in 2014–2015 was greater than that of 0 % for DMPP estimated from manual chamber measurements from 1 October 2014 to 30 September 2015 by Lin et al. (2018), although the reduction modelled in 2014–2016 was similar to that of 38 %, estimated from manual chamber measurements from 1 October 2015 to 30 September 2016.

5.5 Effects of management on seasonal and annual N$_2$O emissions modelled after fall and spring slurry applications

Advancing fall slurry application by 2 weeks increased N$_2$O emissions modelled with and without NI during autumn but reduced those during subsequent spring thaw (F−2 in Table 6) so that annual emissions modelled with and without NI were similar to those in F with the application dates in the experiment (Table 3). Delaying fall slurry application by 2 weeks reduced N$_2$O emissions modelled with and without NI only slightly during autumn but greatly increased emissions modelled during subsequent spring thaw (F+2 in Table 6), particularly with the later fall application in 2016 (Table 3). Consequently delaying fall slurry application by 2 weeks caused substantial increases in annual N$_2$O emissions. However reductions in N$_2$O emissions modelled with NI in F+2 in 2015 and 2016 (34 % and 47 %) were greater than those in F (26 % and 38 %) because inhibition declined

more slowly in colder soil (Eq. 1), particularly with later application in 2016.

Increasing surface litter incorporation and soil mixing during fall slurry application raised N$_2$O emissions modelled without NI only slightly during 2014–2015 but substantially during 2014–2016, particularly during spring thaw (F0.5 and F0.8 vs. F in Table 6). Increasing surface litter incorporation and soil mixing during spring slurry application had limited effects on emissions (S0.5 and S0.8 vs. S in Table 6). Greater mixing caused reductions in N$_2$O emissions modelled with NI to be smaller relative to those without NI.

5.6 NI effects on annual mineral N losses and NH$_3$ emissions

Injecting the slurry to 14 cm in the model suppressed NH$_3$ emissions with limited soil mixing and caused only very small emissions with greater mixing (Table 7). Higher NH$_4^+$ concentrations modelled with NI (Fig. 2a, b) increased net NH$_3$ emissions, particularly if fall slurry application was delayed or soil mixing was increased in 2014–2015.

The subhumid climate at Edmonton (Table 4) caused modelled NO$_3^-$ losses to remain small. For both fall and spring applications, lower NO$_3^-$ concentrations modelled with NI (Fig. 2c, d) caused small reductions in NO$_3^-$ losses.

5.7 NI effects on barley silage yields

Silage yields modelled with fall slurry application were smaller than those measured in the drier year 2015, but those modelled with both applications were greater than those measured in the wetter year 2016, likely because of lodging observed in the field plots following the second year of heavy manure use (Table 8). Modelled yields were unaffected by NI for fall and spring applications in both years, although measured yields were raised by NI with spring application in 2015. Modelled yields were affected by the cutting height and harvest efficiency set in the model runs (Sect. 4.2).

Table 6. Seasonal and annual N_2O emissions modelled during autumn–winter, winter–spring and spring–summer in 2014–2015 and 2014–2016 without slurry (C) or with slurry applied in fall (F) or spring (S) without NI or with R_I for DMPP on dates in the field study (Table 3), in fall on dates 2 weeks before (F−2) or after (F+2) those in the field study, and with soil mixing during slurry application (M) increased to 0.5 and 0.8 from 0.2 in the field study. Negative values denote emissions.

	Year	2014	2015		2014–2015	2015	2016		2015–2016
	From To	16 Sep 31 Dec	1 Jan 30 Apr	1 May 15 Sep	Total	16 Sep 31 Dec	1 Jan 30 Apr	1 May 15 Sep	Total
Treat.	Amend.	mg N m⁻²	mg N m⁻²	mg N m⁻²	mg N m⁻²	mg N m⁻²	mg N m⁻²	mg N m⁻²	mg N m⁻²
C		−2	−10	−14	−26	−2	−11	−13	−26
F	None	−93	−74	−17	−184	−93	−74	−27	−194
F	DMPP	−39	−68	−29	−136	−41	−50	−30	−121
F	Nitrapyrin	−50	−101	−20	−171	−48	−61	−29	−136
S	None	−2	−10	−119	−131	−3	−25	−182	−210
S	DMPP	−2	−10	−90	−102	−3	−18	−106	−127
S	Nitrapyrin	−2	−10	97	−109	−3	−24	−126	−153
F−2	None	−102	−64	−17	−183	−137	−47	−26	−210
F−2	DMPP	−56	−63	−19	−138	−55	−34	−23	−112
F+2	None	−92	−111	−17	−220	−84	−189	−52	−325
F+2	DMPP	−28	−78	−39	−145	−29	−99	−43	−171
F0.5	None	−97	−71	−16	−184	−93	−168	−22	−283
F0.5	DMPP	−58	−77	−17	−152	−59	−111	−20	−190
F0.8	None	−102	−81	−21	−204	−98	−184	−19	−301
F0.8	DMPP	−65	−76	−18	−159	−69	−138	−18	−225
S0.5	None	−2	−10	−129	−141	−3	−27	−168	−198
S0.5	DMPP	−2	−10	−98	−110	−3	−21	−124	−147
S0.8	None	−2	−10	−138	−150	−3	−25	−168	−196
S0.8	DMPP	−2	−10	−102	−114	−3	−19	−123	−145

6   Discussion

6.1   Process modelling of N₂O emissions

N₂O emissions were driven by declines in gaseous O_2 (O_{2g}) and O_{2s} modelled by equilibrating O_2 active uptake by autotrophic and heterotrophic oxidation (Sect. 2.5, step 3, and Sect. 2.3, step 3) with O_2 diffusion and dissolution through gaseous and aqueous phases, and dissolution from gaseous to aqueous phases, largely controlled by θ_g (Fig. 1). These O_2 transfers were sustained by concentration gradients from O_{2g} to O_{2s} and from O_{2s} to O_2 at microbial surfaces (O_{2m}) so that declines in O_{2s} (Fig. 3) and O_{2m} were relatively larger than those in O_{2g}. These greater declines enabled N₂O emissions to be modelled from O_2 deficits, while O_{2g} remained above one-half of atmospheric concentration, consistent with observations of O_{2g} during N₂O emissions from incubation and field experiments (Nguyen et al., 2017; Owens et al., 2017). These O_2 deficits were modelled using a K_m for O_{2m} of 10 μM by nitrifiers (Sect. 2.5, step 3) and 2 μM by denitrifiers (Sect. 2.3, step 3) derived from biochemical studies by Focht and Verstraete (1977). These K_m values are less than

5 % and 1 % of atmospheric equivalent concentration, indicating the importance of explicitly simulating gaseous and aqueous transport processes when modelling N₂O emissions.

O_2 deficits were modelled in spring thaw 2015 (Fig. 3a), when diffusion was sharply reduced by soil saturation because drainage from snowmelt and soil thaw was impeded by underlying ice layers. These declines drove N₂O generation (Fig. 3b) and emission (Fig. 4b) almost entirely from NO_2^- reduced during spring thaw. O_2 deficits were also modelled during winter 2016, when increased θ_i from soil freezing with lower T_s under a shallower snowpack caused near-surface soil porosity to be fully occupied by ice and water. Consequent loss of θ_g greatly reduced surface gas exchange and hence gradually reduced soil O_2 concentrations, particularly with increased O_2 demand from fall slurry application (Fig. 3c). The extended period of low O_{2s} prolonged overwinter accumulation of N_2O_s after fall slurry application (Fig. 3d). Transient increases in θ_g during soil freeze–thaw cycles caused several N₂O emission events to be modelled during spring thaw in 2016, mostly from degassing through volatilization of overwinter N_2O_s (Fig. 5b). De-

Table 7. Annual NO$_3^-$ discharge and NH$_3$ emissions modelled from 16 September to 15 September in 2014–2015 and 2014–2016 without slurry (C) or with slurry applied in fall (F) or spring (S) without NI and with DMPP on dates in the field study (Table 3), in fall on dates 2 weeks before (F−2) or after (F+2) those in the field study, and with soil mixing during slurry application (M) increased to 0.5 and 0.8 from 0.2 in the field study. For NH$_3$ positive values indicate deposition, and negative values indicate emission.

Year		2014–2015		2014–2016	
Treat.	Amend.	NH$_3$ mg N m^{-2}	NO$_3^-$ mg N m^{-2}	NH$_3$ mg N m^{-2}	NO$_3^-$ mg N m^{-2}
C		+14	277	+34	421
F	None	+7	330	+29	691
F	DMPP	−147	317	+13	662
S	None	+8	279	+21	617
S	DMPP	+4	279	+14	598
F−2	None	+4	336	+26	678
F−2	DMPP	−9	326	+12	658
F+2	None	+3	336	+28	697
F+2	DMPP	−194	321	+10	662
F0.5	None	−9	321	+17	558
F0.5	DMPP	−79	314	−3	554
F0.8	None	−34	500	+1	368
F0.8	DMPP	−101	473	−29	370
S0.5	None	−3	279	+1	490
S0.5	DMPP	−7	279	−8	493
S0.8	None	−15	279	−15	361
S0.8	DMPP	−21	279	−26	365

Table 8. Barley silage yields modelled and measured without slurry (C) or with slurry applied in fall (F) or spring (S) with and without NI applied on dates in the field study (Table 3).
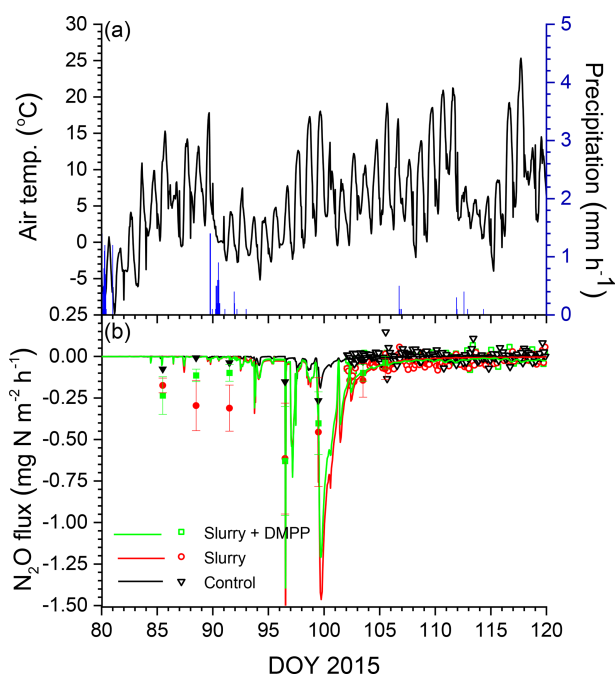
Year		2015		2016	
Treat.	Amend.	Mod. g C m^{-2}	Mes.[a] g C m^{-2}	Mod. g C m^{-2}	Mes.[a,b] g C m^{-2}
C		154	198 ± 24	128	124 ± 9
F	None	284	355 ± 4	344	242 ± 45
F	DMPP	283	360 ± 25	343	255 ± 15
S	None	293	267 ± 12	334	195 ± 33
S	DMPP	297	317 ± 17	344	189 ± 32

[a] Calculated as 45 % dry matter. [b] Measured yields reduced by lodging.

gassing events in the model were consistent with field observations by Chantigny et al. (2017) that passive degassing of accumulated gases made a significant contribution to spring thaw emissions, during which two or more consecutive emission peaks were often observed. In the model, the contribution by degassing of overwinter N$_2$O$_s$ to spring thaw emissions increased with intensity and duration of soil freezing during the previous winter. N$_2$O emissions simulated during spring thaw were thus driven by concurrent NO$_2^-$ reduction during spring thaw (2015) and by earlier NO$_2^-$ reduction accumulated over the previous winter (2015–2016), as has been proposed from experimental observations (Teepe et al., 2004).

O$_2$ deficits were also caused by rapid increases in O$_2$ active uptake with addition of labile C in slurry, the rapid decomposition and oxidation of which (Sect. 2.3, step 1) caused transient declines in O$_{2s}$ with soil wetting from slurry application and precipitation (Fig. 3e, g). After slurry application in the wetter spring of 2016, modelled O$_{2g}$ declined to around one-half of atmospheric concentration, driving the sharp declines in O$_{2s}$ shown in Fig. 3g. The modelled declines in O$_{2g}$ were consistent with results from an incubation of wetted soil amended with cattle slurry by Nguyen et al. (2017), in which O$_{2g}$ declined below one-half of atmospheric concentration within 1 d of slurry application and gradually rose again after 2 d, while no decline occurred in an unamended soil. The period of low O$_{2s}$ in this incubation study coincided with peak emissions of CO$_2$ and N$_2$O from the amended soil, as was modelled here in Figs. 3f, h, 6b and 7b. This coincidence indicated that NH$_4^+$ and DOC oxidation drove O$_2$ deficits from demand for O$_2$ from oxidation vs. supply of O$_2$ through
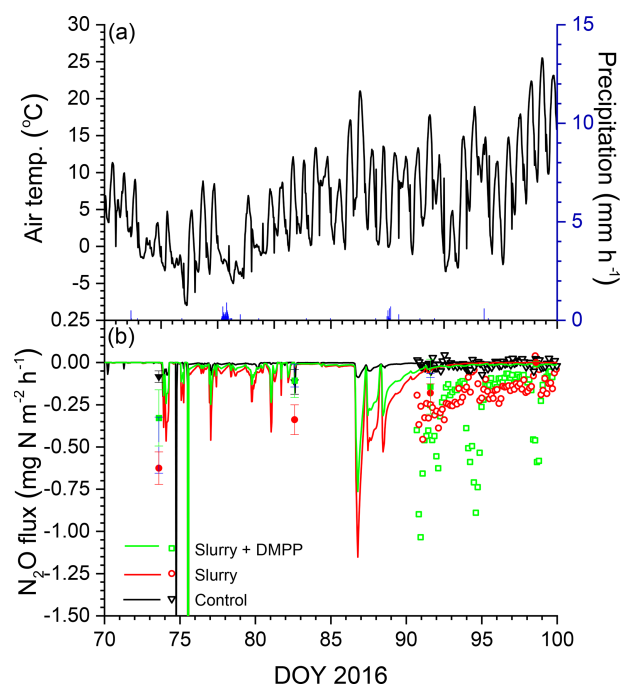
Figure 4. (a) Air temperature and precipitation and **(b)** N$_2$O fluxes measured (symbols) and modelled (lines) during early spring 2015 with no slurry (control) and following slurry application on DOY 273 in 2014 with or without DMPP. Filled symbols represent manual chamber measurements by Lin et al. (2018). Negative values denote emissions.

Figure 5. (a) Air temperature and precipitation and **(b)** N$_2$O fluxes measured (symbols) and modelled (lines) during early spring 2016 with no slurry (control) and following slurry application on DOY 280 in 2015 with or without DMPP. Filled symbols represent manual chamber measurements. Negative values denote emissions.

convection–dispersion, which caused NO$_2^-$ reduction as represented in the model, again demonstrating the importance of simulating aqueous and gaseous O$_2$ transfers when modelling N$_2$O emissions.

6.2 Process modelling of NI effects on N$_2$O emissions

6.2.1 Fall slurry application

NH$_4^+$ oxidation in the model (Sect. 2.5, step 4) proceeded rapidly after fall slurry application without NI, as indicated by rapid declines in NH$_4^+$ (Fig. 2a), consistent with observations in other studies that soil NH$_4^+$ concentrations returned to background levels 30 d after fall slurry application (Rochette et al., 2004). Slower NH$_4^+$ oxidation modelled with NI (Eq. 3) during fall caused slower declines of soil NH$_4^+$ before and during freezing and hence larger NH$_4^+$ concentrations during spring thaw (Fig. 2a). These slower declines were modelled from slower decline of I_t with low f_{T_s} in cold soils (Eq. 1), which slowed NH$_4^+$ oxidation and thereby reduced N$_2$O emissions simulated during late autumn and spring thaw (Figs. 4b and 5b), despite increased NH$_4^+$ concentrations (Fig. 2). These reductions were consistent with those from chamber measurements at the Edmonton South Campus Farm (Lin et al., 2018) and with those from a limited number of studies elsewhere, in which persistent effects
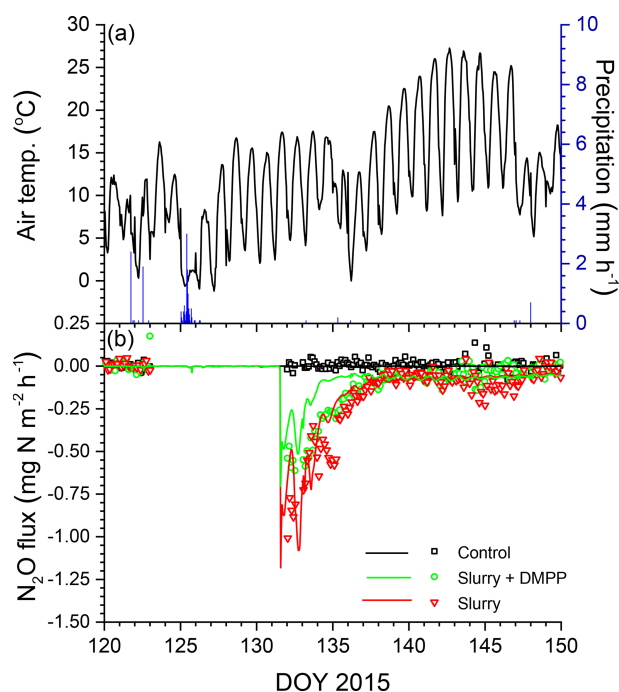
of NI in reducing overwinter N$_2$O emissions have been found (e.g. Pfab et al., 2012), indicating the importance of f_{T_s} in Eq. (1).

The slower decline of I_t from low f_{T_s} enabled ecosys to simulate larger reductions in N$_2$O emissions with NI after fall slurry applications in cooler soil vs. spring slurry applications in warmer soil during both years (F during autumn vs. S during late spring–summer in Table 6). Reductions in N$_2$O emissions modelled with NI after fall slurry applications became greater when fall applications were delayed (F+2 in Table 6), further reducing T_s and f_{T_s} during subsequent nitrification. The greater reductions modelled with fall applications were consistent with experimental observations by Merino et al. (2005), who attributed larger reductions in N$_2$O emissions measured with NI from fall-applied vs. spring-applied cattle slurry to slower NI degradation in cooler soil. These modelled and experimental results indicated that NI effectiveness in reducing N$_2$O emissions varies with the effect of fall slurry timing on f_{T_s}.
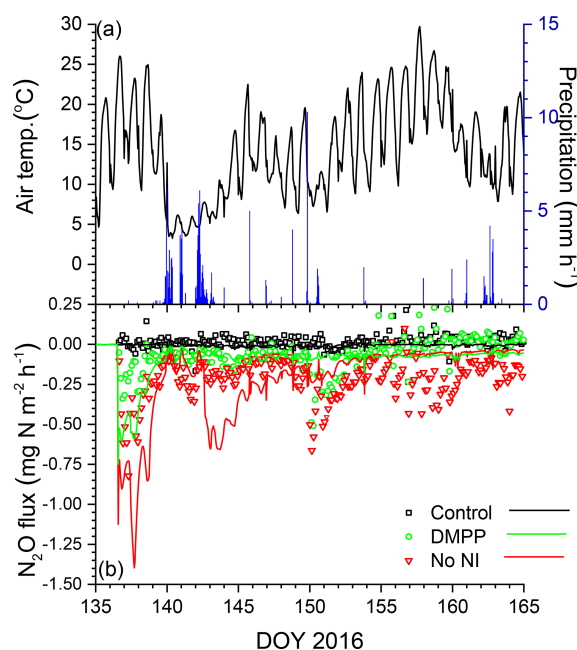
The greater reductions in N$_2$O emissions modelled from delayed fall applications with NI were associated with much greater N$_2$O emissions modelled from delayed fall applications without NI (F+2 in Table 6). These greater emissions were attributed to less NH$_4^+$ oxidation before freeze-up in fall, resulting in more NH$_4^+$ remaining to drive NH$_4^+$ oxidation and hence N$_2$O emissions during spring thaw.

Figure 6. (a) Air temperature and precipitation and **(b)** N$_2$O fluxes measured (symbols) and modelled (lines) during spring 2015 with no slurry (control) and following slurry application on DOY 132 in 2015 with or without DMPP. Negative values denote emissions.

Figure 7. (a) Air temperature and precipitation and **(b)** N$_2$O fluxes measured (symbols) and modelled (lines) during spring 2016 with no slurry (control) and following slurry application on DOY 137 in 2016 with or without DMPP. Negative values denote emissions.

These model findings were consistent with field results from Chantigny et al. (2017) in Quebec and Kariyapperuma et al. (2012) in Ontario, where greater spring N$_2$O emissions were measured when fall slurry was applied in late November than in early November. These greater spring thaw N$_2$O emissions were attributed by Kariyapperuma et al. (2012) to greater mineral N concentrations during spring thaw caused by less nitrification before freeze-up during the previous fall, as modelled here. The greater N$_2$O emissions modelled with later slurry application were also driven by more rapid DOC oxidation from more labile manure C remaining during spring thaw. This more labile manure C reduced [O$_{2s}$] below that simulated after earlier fall applications (Fig. 3d). NI may therefore be particularly effective in reducing N$_2$O emissions during spring thaw following late fall slurry applications.

The decreases in N$_2$O emissions modelled with NI from greater soil mixing (F0.5 and F0.8 vs. F in Table 6) were affected by how the redistribution of NI activity with soil mixing was modelled. Simulating this redistribution during tillage requires further consideration and corroboration from observations. These decreases in N$_2$O emissions with NI were associated with greater N$_2$O emissions modelled from greater soil mixing without NI in 2016 (F0.5 and F0.8 in Table 6). These greater emissions were attributed in the model to longer periods with high θ_i and low θ_g in the upper soil profile caused by greater heat loss through reduced insulation from less surface litter under a shallow snowpack [D12,

D13]. This longer period further reduced overwinter [O$_{2s}$] from that modelled in F (Fig. 3c), causing greater accumulation of N$_2$O$_s$ and hence greater emissions during thaw. These model findings were consistent with field observations by Congreves et al. (2017) and Wagner-Riddle et al. (2010) that overwinter N$_2$O emissions increased with greater freezing under conventional tillage vs. no tillage, particularly with surface residue removal. Model findings were also consistent with observations by Teepe et al. (2004) that N$_2$O emissions during soil thawing rose sharply with increased duration of soil freezing. Consequent changes in T_s with freezing may alter NI effectiveness with tillage.

6.2.2 Spring slurry application

Annual N$_2$O emissions modelled without NI from spring applications were smaller than those from fall applications in 2014–2015, with a wetter early spring and drier late spring, and slightly greater in 2015–2016, with a drier early spring and wetter late spring (Table 4), except when fall application was delayed (e.g. F+2 in Table 6). These modelled differences in emissions were consistent with experimental findings that drier springs reduce N$_2$O emissions from fall applications relative to those from spring (e.g. Cambareri et al., 2017). These model results indicate that effects of spring vs. fall slurry applications on annual N$_2$O emissions may not be consistent but rather will depend on the timing of fall application relative to freeze-up and on precipitation during the following winter and spring.

Amendment of slurry with NI slowed declines in NH$_4^+$ modelled after spring applications comparably to those measured (Fig. 2b). These slower declines were caused by slower NH$_4^+$ oxidation that reduced nitrifier growth (Sect. 2.9, Eq. 3) and active O$_2$ uptake (Sect. 2.5, step 3). Consequently smaller nitrifier biomass and greater [O$_{2s}$] were modelled with NI vs. without NI (Fig. 3e, g), particularly with rainfall after spring application in 2016 (Fig. 7a). The smaller nitrifier biomass modelled with NI was consistent with the findings of Dong et al. (2013) that DMPP reduced populations of ammonia oxidizing bacteria in soil incubations. Greater [O$_{2s}$] modelled with NI was consistent with greater [O$_{2g}$] measured in an incubation of wetted soil amended with cattle slurry with DMPP vs. without DMPP by Nguyen et al. (2017). Slower nitrifier growth and greater [O$_{2s}$] both contributed to reductions in N$_2$O emissions modelled with NI beyond those from the direct effects of I_t on nitrification in Eq. (1), indicating additional effects of NI on N$_2$O emissions that should be considered in NI models.

The reductions in N$_2$O emissions modelled for 30 d after spring slurry applications with R_I for DMPP and nitrapyrin in 2015 (35 % and 30 %) and 2016 (53 % and 41 %) were less than those measured with automated chambers (Table 5) but within the range of 31 % to 44 % in meta-analyses of NI research by Akiyama et al. (2010) and Ruser and Schultz (2015). The greater reductions modelled in 2016 vs. 2015 (Fig. 7 vs. Fig. 6) were consistent with findings in meta-analyses by Akiyama et al. (2010) and Gilsanz et al. (2016) that NI was more effective in reducing N$_2$O emissions from a given land use when emissions were greater. These greater reductions were attributed in the model to heavy rainfall several days after application in 2016 (Fig. 7a) that extended the N$_2$O emission period (Fig. 7b). During this extension I_t remained high because [NH$_4^+$] had declined from the large values modelled immediately after application (Eq. 3).

The effects of NI on N$_2$O emissions modelled with greater soil mixing during spring applications (S0.5 and S0.8 vs. S in Table 6) were affected by how the redistribution of NI activity with soil mixing was modelled, as were those during fall applications. The effects of soil mixing on N$_2$O emissions without NI modelled from slurry applications in spring were smaller than those in fall in the absence of soil freezing effects on O$_{2s}$. These smaller effects were modelled because tillage in this study involved mixing of injected manure rather than incorporation of surface-applied manure. These small effects were consistent with an observation by VanderZaag et al. (2011) that tillage was less important than timing and placement for N$_2$O emissions from slurry applications.

The reductions in annual N$_2$O emissions modelled after spring slurry applications with R_I for DMPP and nitrapyrin in 2015 (22 % and 17 %) and 2016 (40 % and 27 %; Table 6) were smaller than those modelled after 30 d (Table 5) due to gradual degradation of NI effectiveness modelled with time since application (Eq. 1), indicating the importance of year-round modelling and measurements to fully assess NI effects on N$_2$O emission factors for IPCC Tier 3 methodology. However most of the datasets used in meta-analyses of these assessments did not include emissions during autumn, winter and spring thaw (Ruser and Schulz, 2015). which are particularly important for estimating emission factors for NI effects from fall slurry applications in cold climates (Table 6). An ecosystem modelled with well-tested simulation of NI effects may make a valuable contribution to these assessments.

6.3 Modelling NI effects on NH$_3$ emissions and mineral N losses

The small NH$_3$ emissions modelled from slurry injection with limited soil mixing (Table 7) were consistent with observations of almost no NH$_3$ volatilization from closed-slot injection of slurry by Rodhe et al. (2006). In the model, NH$_3$ emissions with or without NI were sharply reduced by NH$_4^+$ adsorption with diffusion of NH$_3$ and NH$_4^+$ from the injection site. Greater soil mixing brought more NH$_4^+$ closer to the surface, reducing NH$_4^+$ adsorption and thereby increasing NH$_3$ emission, particularly from fall applications with NI (Table 7). Consequently only small net increases in NH$_3$ emissions (Table 7) were modelled with NI from increased volatilization of aqueous NH$_3$ in equilibrium with increased NH$_4^+$ concentrations (Fig. 2). However these increases were large in relative terms, particularly following fall applications, consistent with increases of 33 %–67 % and 3 %–65 % relative to emissions without NI derived from meta-analyses of field experiments by Qiao et al. (2015) and Lam et al. (2017) respectively. Increases in NH$_3$ emissions with NI will thus depend on soil adsorptive properties and depth of slurry incorporation.

The small losses of NO$_3^-$, and consequently the small reductions in these losses with NI, modelled in the subhumid climate at the Edmonton South Campus Farm (Table 7) conform to the assumption by De Klein et al. (2006) that NO$_3^-$ leaching is an insignificant source of indirect N$_2$O emission from dryland cropping systems in subhumid climates. Consequently reductions in leaching have minimal impact on the overall effect of NI on N$_2$O emission in these climates (Lam et al., 2017). Reductions in NO$_3^-$ losses modelled with NI would be larger at sites with better drainage and more excess precipitation, although even under these conditions such reductions may be small and inconsistent (Smith et al., 2002).

The increases in NH$_3$ emissions modelled with NI were larger than reductions in NO$_3^-$ leaching (Table 7), indicating that net increases in N$_2$O emissions from indirect effects of NI will partially offset decreases in N$_2$O emissions from direct effects. This offset must be included when estimating changes in N$_2$O emission factors attributed to NI in IPCC Tier 3 methodology.

6.4 Modelling NI effects on N$_2$O emissions: parameter evaluation

The simulation of N$_2$O emissions from nitrification and denitrification in ecosys is based on a comprehensive representation of biological and physical processes governing production and transport of N$_2$O. Parameters used in these processes are well constrained from basic research so that the model may provide a robust means to predict emissions under diverse climates, soils and land use practices. These processes in ecosys were not changed when adding the algorithm for inhibiting NH$_4^+$ oxidation by nitrifiers proposed in Eqs. (1) and (2) (Sect. 2.9). This algorithm used only three parameters, $I_{t=0}$ and R_I in Eq. (1) and K_{iNH_4} in Eq. (2), with values of 1.0, 2.0×10^{-4} h^{-1} and 7000 g N m^{-3} to simulate the time course of NI activity following slurry application. The first two parameters correspond to those in earlier models of NI for inhibition effectiveness (0.5–0.9) and duration (30–60 d; Cui et al., 2014; Del Grosso et al., 2009). These models have given reductions in N$_2$O emissions with NI in agricultural crops of around 25 % (Cui et al., 2014), 10 % (Del Grosso et al., 2009) or less (Abalos et al., 2016), which are frequently smaller than reductions of 26 %–43 % and 24 %–46 % derived from meta-analyses of NI effects in agricultural crops by Akiyama et al. (2010) and Gilsanz et al. (2016) respectively. Direct effects on NI of soil water content and pH were not modelled here due to uncertainty in parameterization, although both affect nitrification and hence the magnitude of NI activity.

Each of the parameters used to model NI in ecosys requires further evaluation. A larger R_I, such as that used for nitrapyrin vs. DMPP (Sect. 2.9), caused a more rapid decline of NI activity in soil and hence greater N$_2$O emissions with time after slurry application that were consistent with measurements (Tables 5 and 6; Lin et al., 2018). This larger value might represent more rapid degradation of nitrapyrin through volatilization (Ruser and Schulz, 2015), although meta-analyses of N$_2$O reductions with NI indicate that those with nitrapyrin are similar to those with DMPP. The value of R_I used for NI in the model will thus likely be product specific. The effect of T_s on R_I might reasonably be represented by f_{T_s}, as is the effect of T_s on all other biological reactions in the model. This function allowed modelled NI activity to persist over winter (Fig. 2) and hence reduce N$_2$O emissions modelled during spring thaw (Figs. 6 and 7). However the effects of temperature on reductions in N$_2$O emission with NI over time are sometimes unclear in controlled studies (Kelliher et al., 2008).

The value of $I_{t=0}$ set the value of I_t at the time of slurry application, after which I_t underwent first-order decline over time according to Eq. (1) (Sect. 2.9). The current value of 1.0 indicates complete inhibition at the time of application but might be reduced if the amount of NI at application is less than that required for complete inhibition. However I_t had to remain large enough to reduce N$_2$O emissions from

Table 9. Sensitivity of seasonal N$_2$O emissions modelled during late spring in 2015 and 2016 to changes in initial inhibition ($I_{t=0}$ in Eq. 1) and inhibition constant (K_{iNH_4} in Eq. 2) following spring slurry application on dates in the field study (Table 3). Negative values denote emissions.

Year		2015	2016
Period		12 May–11 Jun mg N m^{-2}	17 May–16 Jun mg N m^{-2}
No NI	No NI	−89*	−153*
$I_{t=0}$	K_{iNH_4}		
1.0	7000	−58*	−72*
0.9	7000	−60	−80
0.8	7000	−62	−90
1.0	3500	−62	−78
0.9	3500	−64	−86
0.8	3500	−65	−95
1.0	14 000	−54	−66
0.9	14 000	−57	−75
0.8	14 000	−59	−85

* From Table 5.

nitrification for several weeks after application (Figs. 6 and 7) even with higher soil NH$_4^+$ concentrations (Fig. 2). Lowering $I_{t=0}$ from 1.0 to 0.8, similar to that in earlier NI models in which I_t decline was not simulated, increased N$_2$O emissions modelled over 30 d after spring slurry applications by 7 % in 2015 and 25 % in 2016 (Table 9).

The value of K_{iNH_4} in Eq. (2) reduced I_t with the very large NH$_4^+$ concentrations modelled immediately after injecting slurry with large NH$_4^+$ content (Table 3) into small bands (Sect. 3.1). The use of K_{iNH_4} was suggested by the findings of Janke et al. (2019) that NI may not have the expected impacts on N transformations and availability when applied in a concentrated band with large NH$_4^+$ concentrations (up to 12 kg N Mg^{-1}), similar to those modelled immediately after slurry application in this study. The modelled NH$_4^+$ concentrations declined rapidly after application through diffusion, adsorption and nitrification (Sect. 2.5), and thus so did K_{iNH_4} effects on inhibition. The value of K_{iNH_4} in Eq. (2) therefore governed NI effects modelled during the brief periods of rapid N$_2$O emissions following application (around 3 d in Figs. 6 and 7) but had sharply diminishing impacts on NI effects modelled thereafter. An alternative hypothesis for reduced inhibition by NI immediately after application might be more rapid diffusion of NH$_4^+$ than NI from the band, leading to spatial separation (Ruser and Schulz, 2015), although parameterization of this hypothesis is uncertain. Halving or doubling K_{iNH_4} from the value set in Sect. 2.9 raised or lowered N$_2$O emissions modelled over 30 d after spring slurry applications by 7 %–8 % in 2015 and 2016 (Table 9), indicating some latitude in evaluating this parameter.

Reductions in N$_2$O emissions modelled with all proposed values of $I_{t=0}$ and K_{iNH_4} varied from 27 % to 41 % in 2015, and from 38 % to 57 % in 2016 (Table 9), close to the range of 42.6 % ± 5.5 % derived from meta-analyses of NI effects with cattle slurry by Gilsanz et al. (2016). Further evaluation of these parameters should be undertaken in future studies in which measurements are taken at higher frequencies (e.g. Figs. 6 and 7) required to assess N$_2$O emissions and NI effects on them.

6.5 Modelling NI effects on N$_2$O emissions: outstanding issues

Several issues remain to be addressed in modelling N$_2$O emissions and NI effects on these emissions. Accurately modelling emissions during spring thaw depended upon accurately modelling soil freezing and thawing following snowmelt and their effects on soil O$_2$ transfer. A small delay of 2–3 d in modelled thawing caused some small emission events measured in early spring of 2015 to be missed (Fig. 4b). However because modelled emissions were driven by overwinter accumulation of N$_2$O (Fig. 3), seasonal emissions were less affected by such delays than emissions from individual events. Algorithms for modelling snowpack accumulation and ablation in ecosys are being further refined to improve simulation of soil freezing and thawing. Accurately modelling emissions later in spring depended upon accurately modelling soil wetting and drying following rainfall and their effects on soil O$_2$ transfer. Soil wetting from heavy precipitation typically drives N$_2$O emission events following soil N additions, as modelled here during DOY 143–146 in 2016, although such events were not always measured (Fig. 7b). Such wetting caused sharp declines in O$_{2s}$ when soil water content rose above a critical threshold, driving N$_2$O generation and subsequent emission (Fig. 3). However modelling these thresholds depends on soil hydrological properties used in the model (Table 2) which may not be known with sufficient accuracy.

Modelling NI effects on N$_2$O emissions depended not only upon $I_{t=0}$ (Eq. 1) and K_{iNH_4} (Eq. 2) as evaluated in Sect. 6.4 and Table 9 but also upon the time course for declining NI activity governed by the first-order rate constant R_I and its temperature dependence $f_{T_{s_l}}$ (Eq. 1). NI activity modelled with R_I and $f_{T_{s_l}}$ in this study reduced nitrification alone (Sect. 2.9), which enabled higher [NH$_4^+$] and lower [NO$_3^-$], and hence greater NH$_3$ emissions, to be simulated with NI after amendment, as has been found in field studies (Fig. 2). These higher [NH$_4^+$] required a low value of R_I so that NI activity would persist in reducing nitrification and hence N$_2$O emissions after soil amendment. This model of NI activity contrasted with that in a more complex model in which NI reduced N$_2$O emissions directly rather than through nitrification (Li et al., 2020). In such a model, NI would not directly affect [NH$_4^+$] and [NO$_3^-$] so that greater values of R_I could be used to get similar reductions in N$_2$O emissions. The val-

ues of R_I and $f_{T_{s_l}}$ used in our model caused N$_2$O emissions modelled with NI to decline more rapidly than those measured following spring applications (Figs. 6b and 7b). These values need to be constrained by further studies with more frequent measurements of declines in NI activity following amendment to determine if alternative models for the time course of these declines might be considered.

7 Conclusions

Findings from this modelling study may be summarized as follows:

a. A simple, time-dependent algorithm for adding NI effects on N$_2$O emissions into the existing model ecosys was presented.

b. The direct effect of NI on N$_2$O emissions in the model was confined to the inhibition of NH$_4^+$ oxidation.

c. Additional effects of NI on N$_2$O emissions were caused by slower nitrifier growth and O$_2$ uptake. The combined effects in (b) and (c) reduced N$_2$O emissions by 35 %–58 % depending on seasonal weather and time of manure application.

d. Slower nitrification modelled with this algorithm caused increases in soil NH$_4^+$ concentrations and reductions in soil NO$_3^-$ concentrations and N$_2$O fluxes that were consistent with those measured following fall and spring applications of slurry over 2 years.

e. NI in the model remained effective in reducing N$_2$O emissions modelled during spring thaw, particularly when these emissions were increased by delaying fall slurry applications or increasing fall tillage intensity.

f. NI in the model increased NH$_3$ emissions more than they reduced NO$_3^-$ leaching, causing indirect effects on N$_2$O emissions that partially offset direct effects.

g. NI had no significant effect on modelled or measured barley silage yields.

h. Some further work is needed to corroborate parameters in the NI algorithm under a wider range of site conditions.

i. The addition of NI to ecosys may allow emission factors for different NI products to be derived from annual N$_2$O emissions modelled under diverse site, soil, land use and weather, as required in IPCC Tier 3 methodology.

References

Abalos , D., Smith, W. N., Grant, B. B., Drury, C. F., MacKell, S., and Wagner-Riddle, C.: Scenario analysis of fertilizer management practices for N_2O mitigation from corn systems in Canada, Sci. Total Environ., 573, 356–365, 2016.

Akiyama, H., Yan, X., and Yagi, K.: Evaluation of effectiveness of enhanced efficiency fertilizers as mitigation options for N_2O and NO emissions from agricultural soils: Meta-analysis, Glob. Change Biol., 16, 1837–1846, https://doi.org/10.1111/j.1365-2486.2009.02031.x, 2010.

Cambareri, G., Drury, C., Lauzon, J., Salas, W., and Wagner-Riddle, C.: Year-round nitrous oxide emissions as affected by timing and method of dairy slurry application to corn, Soil Sci. Soc. Am. J., 81, 166–178, 2017.

Chantigny, M. H., Rochette, P., Angers, D. A., Goyer, C., Brin, L. D., and Bertrand, N.: Nongrowing season N_2O and CO_2 emissions – Temporal dynamics and influence of soil texture and fall-applied slurry, Can. J. Soil Sci., 97, 452–464, 2017.

Congreves, K. A., Brown, S. E., Németh, D. D., Dunfield K. E., and Wagner-Riddle, C.: Differences in field-scale N_2O flux linked to crop residue removal under two tillage

systems in cold climates, GCB Bioenergy, 9, 666–680, https://doi.org/10.1111/gcbb.12354, 2017.

Cui, F., Zheng, X., Liu, C., Wang, K., Zhou, Z., and Deng, J.: Assessing biogeochemical effects and best management practice for a wheat–maize cropping system using the DNDC model, Biogeosciences, 11, 91–107, https://doi.org/10.5194/bg-11-91-2014, 2014.

De Klein, C., Novoa, R. S. A., Ogle, S., Smith, K. A., Rochette, P., Wirth, T. C., McKonkey, B. G., Mosier, A., and Rypdal, K.: N_2O emissions from managed soils, and CO_2 emissions from lime and urea application, chap. 11, in: 2006 IPCC Guidelines for National Greenhouse Gas Inventories, edited by: Eggleston, H. S., Buendia, L., Miwa, K., Ngara, T., and Tanabe, K., IGES, Hayama, Japan, 2006.

Del Grosso, S. J., Ojima, D. S., Parton, W. J., Stehfest, E., Heistemann, M., DeAngelo, B., and Rose, S.: Global scale DAYCENT model analysis of greenhouse gas emissions and mitigation strategies for cropped soils, Glob. Planet. Change, 67, 44–50, 2009.

Dong, X. X., Zhang, L. L., Wu, Z. J., Zhang, H. W., and Gong, P.: The response of nitrifier, N-fixer and denitrifier gene copy numbers to the nitrification inhibitor 3,4-dimethylpyrazole phosphate Plant, Soil Environ., 59, 398–403, 2013

Dungan, R. S., Leytem, A. B., Tarkalson, D. D., Ippolito, J. A., and Bjorneberg, D. L.: Dairy forage rotation as influenced by fertilizer and slurry applications, Soil Sci. Soc. Amer. J., 81, 537–545, 2017.

Focht, D. D. and Verstraete, W.: Biochemical ecology of nitrification and denitrification, Adv. Micro. Ecol., 1, 135–214, 1977.

Gao, W. and Bian, X.: Evaluation of the agronomic impacts on yield-scaled N_2O emission from wheat and maize fields in China, Sustainability, 9, 1201, https://doi.org/10.3390/su9071201, 2017.

Gilsanz, C., Báez, D., Misselbrook, T. H., Dhanoa, M. S., and Cárdenas, L. M.: Development of emission factors and efficiency of two nitrification inhibitors, DCD and DMPP, Agric, Ecosyst. Environ., 216, 1–8, 2016.

Giltrap, D. L., Saggar, S., Singh, J., Harvey, M., McMillan, A., and Laubach, J.: Field-scale verification of nitrous oxide emission reduction with DCD in dairy-grazed pasture using measurements and modelling, Soil Res., 49, 696–702, https://doi.org/10.1071/SR11090, 2011.

Grant, R. F.: A technique for estimating denitrification rates at different soil temperatures, water contents and nitrate concentrations, Soil Sci., 152, 41–52, 1991.

Grant, R. F.: Simulation of ecological controls on nitrification, Soil Biol. Biochem., 26, 305–315, 1994.

Grant, R. F.: Mathematical modelling of nitrous oxide evolution during nitrification, Soil Biol. Biochem., 27, 1117–1125, 1995.

Grant, R. F. and Pattey, E.: Mathematical modelling of nitrous oxide emissions from an agricultural field during spring thaw, Global Biogeochem. Cy., 13, 679–694, 1999.

Grant, R. F. and Pattey, E.: Temperature sensitivity of N_2O emissions from fertilized agricultural soils: mathematical modelling in *ecosys*, Global Biogeochem. Cy., 22, GB4019, https://doi.org/10.1029/2008GB003273, 2008.

Grant, R. F., Pattey, E. M., Goddard, T. W., Kryzanowski, L. M., and Puurveen, H.: Modelling the effects of fertilizer application

rate on nitrous oxide emissions from agricultural fields, Soil Sci Soc. Amer. J., 70, 235–248, 2006.

Grant, R. F., Neftel, A., and Calanca, P.: Ecological controls on N$_2$O emission in surface litter and near-surface soil of a managed grassland: modelling and measurements, Biogeosciences, 13, 3549–3571, https://doi.org/10.5194/bg-13-3549-2016, 2016.

Guardia, G., Marsden, K. A., Vallejo, A., Jones, D. L., and Chadwick, D. R.: Determining the influence of environmental and edaphic factors on the fate of the nitrification inhibitors DCD and DMPP in soil, Sci. Total Environ., 624, 1202–1212, 2018.

IPCC: Refinement to the 2006 IPCC guidelines for national greenhouse gas inventories, available at: https://www.ipcc.ch/, last access: 9 July 2019.

Janke, C. K., Fujinuma, R., Moody, P., and Bell, M. J.: Biochemical effects of banding limit the benefits of nitrification inhibition and controlled-release technology in the fertosphere of high N-input systems, Soil Res., 57, 28–40, https://doi.org/10.1071/SR18211, 2019.

Kariyapperuma, K. A., Furon, A., and Wagner-Riddle, C.: Nongrowing season nitrous oxide fluxes from an agricultural soil as affected by application of liquid and composted swine slurry, Can. J. Soil Sci., 92, 315–327, 2012.

Kelliher, F. M., Clough, T. J., Clark, H., Rys, G., and Sedcole, J. R.: The temperature dependence of dicyandiamide (DCD) degradation in soils: a data synthesis, Soil Biol. Biochem., 40, 878–1882, 2008.

Lam, S. K., Suter, H., Mosier, A. R., and Chen, D.: Using nitrification inhibitors to mitigate agricultural N$_2$O emission: a double-edged sword?, Glob. Change Biol., 23, 485–489, 2017.

Li, Y., Shah, S. H. H., and Wang, J.: Modelling nitrification inhibitor effects on emissions of nitrous oxide (N$_2$O) in the UK, Sci. Total Environ., 709, 136156, https://doi.org/10.1016/j.scitotenv.2019, 2020.

Lin, S., Hernandez-Ramirez, G., Kryzanowski, L., Wallace, T., Grant, R., Degenhardt, R., Berger, N., Lohstraeter , G., and Powers, L.-A.: Timing of Slurry Injection and Nitrification Inhibitors Impacts on Nitrous Oxide Emissions and Nitrogen Transformations in a Barley Crop, Soil Sci. Soc. Amer. J., 81, 1595–1605 https://doi.org/10.2136/sssaj2017.03.0093, 2018.

Merino, P., Menéndez, S., Pinto, M., González-Murua, C., and Estavillo, J. M.: 3, 4-Dimethylpyrazole phosphate reduces nitrous oxide emissions from grassland after slurry application, Soil Use Manage, 21, 53–57, 2005.

Metivier, K. A., Pattey, E., and Grant, R. F.: Using the *ecosys* mathematical model to simulate temporal variability of nitrous oxide emissions from a fertilized agricultural soil, Soil Biol. Biochem., 41, 2370–2386, 2009.

Nguyen, Q. V., Wu, D., Kong, X., Bol, R., Petersen, S. O., Jensen, L. S., Liu, S., Brüggemann, N., Glud, R. N., Larsen, M., and Bruun, S.: Effects of cattle slurry and nitrification inhibitor application on spatial soil-dynamics and N$_2$O production pathways, Soil Biol. Biochem., 11, 200–209, 2017.

Owens, J., Clough, T. J., Laubach, J., Hunt, J. E., and Venterea, R. T.: Nitrous oxide fluxes and soil oxygen dynamics of soil treated with cow urine, Soil Sci. Soc. Amer. J., 81, 289–298, https://doi.org/10.2136/sssaj2016.09.0277, 2017.

Pfab, H., Palmer, I., Buegger, F., Fiedler, S., Muller, T., and Ruser, R.: Influence of a nitrification inhibitor and of placed N-

fertilization on N$_2$O fluxes from a vegetable cropped loamy soil, Agr. Ecosyst. Environ., 150, 91–101, 2012.

Qiao, C., Liu, L., Hu, S., Compton, J. E., Greaver, T. L., and Li, Q.: How inhibiting nitrification affects nitrogen cycle and reduces environmental impacts of anthropogenic nitrogen input, Glob. Change Biol., 21, 1249–1257, 2015.

Rochette, P., Angers, D. A., Chantigny, M. H., Bertrand, N., and Côté, D.: Carbon dioxide and nitrous oxide emissions following fall and spring applications of pig slurry to an agricultural soil, Soil Sci. Soc. Amer. J., 68, 1410–1420, 2004.

Rodhe, L., Pell, M., and Yamulki, S.: Nitrous oxide, methane and ammonia emissions following slurry spreading on grassland, Soil Use Manage., 22, 229–237, https://doi.org/10.1111/j.1475-2743.2006.00043.x, 2006.

Ruser, R. and Schulz, R.: The effect of nitrification inhibitors on the nitrous oxide (N$_2$O) release from agricultural soils – a review, J. Plant Nutr. Soil Sci., 178, 171–188, 2015.

Saxton, K. E., Rawls, W. J., Romberger, J. S., and Papendick, R. I.: Estimating generalized soil-water characteristics from texture, Soil Sci. Soc. Amer. J., 50, 1031–1036, 1986.

Smith, K. A., Beckwith, C. P., Chalmers, A. G., and Jackson, D. R.: Nitrate leaching following autumn and winter application of animal manures to grassland, Soil Use Manage., 18, 428–434, 2002.

Subbarao G. V., Ito, O., Sahrawat, K. L., Berry, W. L., Nakahara, K., Ishikawa, T., Watanabe, T., Suenaga, K., Rondon, M., and Rao, I. M.: Scope and strategies for regulation of nitrification in agricultural systems: challenges and opportunities, Crit. Rev. Plant Sci., 25, 303–335, 2006.

Teepe, R., Vor, A., Beese, F., and Ludwig, B.: Emissions of N$_2$O from soils during cycles of freezing and thawing and the effects of soil water, texture and duration of freezing, Euro. J. Soil Sci., 55, 357–365, 2004.

VanderZaag, A. C., Jayasundara, S., and Wagner-Riddle, C.: Strategies to mitigate nitrous oxide emissions from land applied manure, Animal Feed Sci. Tech., 166/167, 464–479, 2011.

Wagner-Riddle, C. and Thurtell, G. W.: Nitrous oxide emissions from agricultural fields during winter and spring thaw as affected by management practices, Nutr. Cycl. Agroecosyst., 52, 151–163, 1998.

Wagner-Riddle, C., Rapai, J., Warland, J., and Furon, A.: Nitrous oxide fluxes related to soil freeze and thaw periods identified using heat pulse probes, Can. J. Soil Sci., 90, 409–418, 2010.

Zhu, K., Bruun, S., and Jensen, L. S.: Nitrogen transformations in and N$_2$O emissions from soil amended with slurry solids and nitrification inhibitor, Euro. J. Soil Sci., 67, 792–803, 2016.